A reliable progressive fatigue damage model for life prediction of composite laminates incorporating an adaptive cyclic jump algorithm

Zheng, Tao; Guo, Licheng; Wang, Zhenxin; Benedictus, Rinze; Pascoe, John Alan

DOI
10.1016/j.compscitech.2022.109587

Publication date
2022

Document Version
Final published version

Published in
Composites Science and Technology

Composites Science and Technology 227 (2022) 109587

Contents lists available at ScienceDirect

Composites Science and Technology

journal homepage: www.elsevier.com/locate/compscitech

A reliable progressive fatigue damage model for life prediction of composite laminates incorporating an adaptive cyclic jump algorithm

Tao Zheng [a,b], Licheng Guo [a,*], Zhenxin Wang [c], Rinze Benedictus [b], John-Alan Pascoe [b]

[a] Department of Astronautic Science and Mechanics, Harbin Institute of Technology, Harbin, 150001, PR China
[b] Structural Integrity and Composites Group, Faculty of Aerospace Engineering, Delft University of Technology, the Netherlands
[c] AECC Commercial Aircraft Engine Co, LTD, Shanghai, 201108, China

ARTICLE INFO

Keywords:
A. polymer-matrix composites (PMCs)
A. Laminate
B. Fatigue
C. Finite element analysis (FEA)
D. Life prediction

ABSTRACT

In this paper, a reliable progressive fatigue damage model (PFDM) for predicting the fatigue life of composite laminates is proposed by combining the normalized fatigue life model, nonlinear residual degradation models and fatigue-improved Puck criterion. To balance the accuracy of life predictions and computational efficiency, an adaptive cyclic jump algorithm is developed and implemented within the PFDM. The sensitivity of life prediction to cyclic jump parameter has been greatly reduced by correlating the cyclic jump with the increment time and viscous coefficient. Therefore, the cyclic jump parameter can be arbitrarily selected within a relatively large range to obtain convergent results. When incorporating the adaptive cyclic jump algorithm, there is no need to define a standard for determining the material failure in numerical calculations, which effectively eliminates an artificially induced uncertainty in life predictions. Two sets of experiments are conducted to validate the proposed PFDM. The numerical predictions including static failure strength and fatigue life correlate reasonably well with the available experimental data.

1. Introduction

Fiber-reinforced composites are widely used in transportation, aviation and aerospace fields because of their exceptional performances including high specific strength, favorable fatigue resistance and corrosion resistance [1]. However, composite structures are generally exposed to series of cyclic fatigue loadings during their service life, and fatigue-induced failure has become one of the most common damage modes. Compared with traditional homogenous materials, the fatigue damage mechanisms of composites are much more complicated due to the various damage modes including delamination, fiber breakage, interface debonding and matrix crack [2]. The complexity and diversity of damage mechanism make it difficult to develop a unified and comprehensive theory to fully characterize the fatigue failure behaviors of laminated composites. Numerous modeling methodologies have been developed to predict the fatigue life of composite laminates over the past few decades. A comprehensive classification of these approaches has been reported by Degrieck et al. [3]. According to the classification, the available fatigue models can be classified into three main categories: fatigue life model (FLM), residual phenomenological model (RPM), and progressive fatigue damage model (PFDM). Although FLM [4–6] and RPM [7–12] models are convenient and efficient for engineering application, they do not consider the actual damage accumulations and therefore cannot be adopted to investigate the fatigue failure behaviors of composites.

In contrast to FLM and RPM models, PFDM models take into account the local stress distributions and physical fatigue damage mechanisms inside the composite structures. Comprehensive failure criteria are required to identify the various damage modes of composites in PFDM, and residual degradation models are implemented to capture the gradual fatigue-induced deterioration. Shokrieh and Lessard [13] initially proposed a generalized PFDM to predict the fatigue life and residual properties of composite laminates. Based on Shokrieh's model, Diao et al. [14] proposed a statistical fatigue damage model. Subsequently, Tserpes et al. [15] studied the damage accumulations of composites under tension-compression cyclic loading by incorporating the PFDM technique. Lian and Yao [16] conducted a FEA simulation to predict the fatigue damage accumulations of laminated composites, and the material properties were assumed to follow a normal distribution function. Recently, the PFDM approach has been successfully applied to investigate the fatigue failure behaviors of composite heterostructures, including notched composite rings [17], full-scale composite cabin [18]

* Corresponding author.
E-mail address: guolc@hit.edu.cn (L. Guo).

https://doi.org/10.1016/j.compscitech.2022.109587
Received 7 March 2022; Received in revised form 28 May 2022; Accepted 8 June 2022
Available online 11 June 2022

and high-speed composite craft [19]. However, most of the above models employed a sudden-discount approach to degrade the properties once the failure criteria are activated, which is too empirical and may result in strong mesh dependency for numerical predictions [20,21].

It should be noted that in numerical calculations, it is impractical to update the damage status and stress distribution cycle by cycle due to the huge computational cost. To solve this problem, the cycle jump approach is introduced [22], which updates the internal variables of FE models at predefined interval cycles. In order to balance the accuracy of life predictions and computational efficiency, it is critical to choose the appropriate cyclic jump. The simplest approach is to predefine the cyclic jump as a constant [23–25]. Similarly, Xu et al. [26] proposed an exponential cyclic jump method, with which the numerical calculations are conducted at cycle numbers $N = 10^{0.25i}$. Guo et al. [24] have studied the influence of cyclic jump on the predicted fatigue life of 3D woven composites. It was found that the predicted life and residual stiffness are extremely sensitive to the chosen increment if the cycle jump is kept constant. Moreover, the exponential cyclic jump method [26] was also indicated to be inapplicable for Guo's fatigue damage model because cyclic jump increases exponentially with the number of cycles, which increases the chances of overshooting the point at which sudden failure occurs. In contrast to predefining the cyclic jump, an automatic cyclic jump algorithm has been developed by Van Paepegem et al. [22]. The local cyclic jump of each integration point was first calculated by imposing a maximum damage increment, then the global cyclic jump can be determined by analyzing the cumulative statistical distribution of all local cyclic jumps. Rivera et al. [27] and Llobet et al. [28] then integrated the automatic cyclic jump algorithm into PFDM to predict fatigue life. However, an error in simulations of these models will be induced by the extrapolation of internal variables, which may be prohibitive for life prediction according to Sally et al. [29]. Moreover, it is also complicated to collect the information of all integration points for the numerical implementation of the automatic cyclic jump algorithm. Therefore, a reasonable cyclic jump approach, capable of reducing the sensitivity of life predictions to user inputs, is essential to be developed.

A reliable PFDM model is proposed in this paper to predict the fatigue life of laminated composites by combining the normalized fatigue life model, nonlinear residual stiffness and strength degradation models and the fatigue-improved Puck criterion [30]. The proposed PFDM is numerically implemented through a user defined subroutine UMAT. Several damage variables are defined to capture the different damage modes of composites, and the constitutive equations are subsequently defined in terms of damage variables. An adaptive cyclic jump algorithm is developed and implemented within the PFDM. A parametrical study is then conducted to estimate the sensitivity of life predictions to the cyclic jump parameter of the adaptive algorithm. The model input parameters are derived from tests on specimens with $[0]_{16}$, $[(45/-45)_8]$ and $[90]_{16}$ lay-ups, and multiple specimens of composite laminates with $[45/-45/0/0/-45/90/45/0]_S$ lay-up are then tested to validate the numerical predictions.

2. Progressive fatigue damage model

2.1. Fatigue-improved Puck criterion

Owing to the concept of action plane as displayed in Fig. 1, the Puck criteria [30] can not only determine the locations but also the orientation of transverse cracks. The fiber failure and transverse inter-fiber failure are separately considered by employing four different equations. In this paper, the original Puck criteria [31] have been improved to predict the damage initiations of fatigue-induced failures by introducing the residual strengths. This gives the following four failure criteria φ_k, with failure occurring when $\varphi_k \geq 1$:

Longitudinal fiber tensile failure criterion, when $\sigma_{11} \geq 0$:

$$\varphi_{fft} = \left[\sigma_{11} + m_f\nu_{12}\sigma_{22} + m_f\nu_{13}\sigma_{33}\right] / S_{r,1t}(n) \tag{1}$$

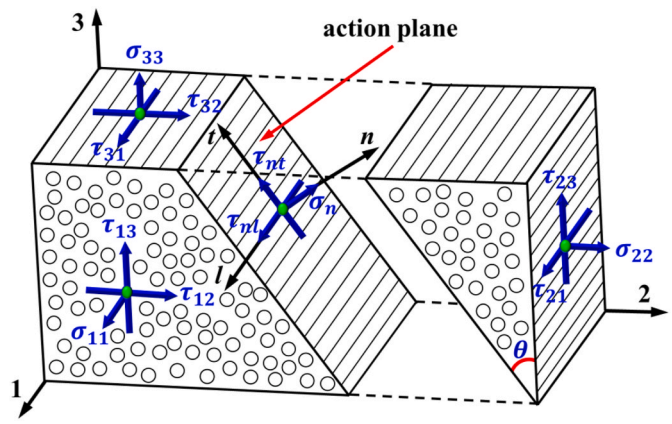

Fig. 1. The transverse action plane of unidirectional lamina subjected to general stresses.

Longitudinal fiber compressive failure, when $\sigma_{11} < 0$:

$$\varphi_{ffc} = -\left[\sigma_{11} + m_f\nu_{12}\sigma_{22} + m_f\nu_{13}\sigma_{33}\right] / S_{r,1c}(n) \tag{2}$$

Transverse inter-fiber tensile failure, when $\sigma_n(\theta) \geq 0$:

$$\varphi_{iff t}(\theta) = \left[\frac{1}{S^2_{r,2t}(n)} - \frac{2P_{\varphi,t}}{S_{r,\varphi}(n)S_{r,2t}(n)}\right]\sigma^2_n(\theta) + 2\frac{P_{\varphi,t}}{S_{r,\varphi}(n)}\sigma_n(\theta) + \frac{\tau^2_{nt}(\theta)}{S^2_{r,23}(n)} + \frac{\tau^2_{nl}(\theta)}{S^2_{r,21}(n)} \tag{3}$$

Transverse inter-fiber compressive failure, when $\sigma_n(\theta) < 0$:

$$\varphi_{iffc}(\theta) = \tau^2_{nt}(\theta)\Big/S^2_{r,23}(n) + \tau^2_{nl}(\theta)\Big/S^2_{r,21}(n) + 2\sigma_n(\theta)P_{\varphi,c}\Big/S_{r,\varphi}(n) \tag{4}$$

where m_f denotes the stress magnification factor caused by different material modulus, $S_{r,1t}(n)$ $S_{r,1c}(n)$, $S_{r,2t}(n)$ and $S_{r,2c}(n)$ are the residual strengths of the single lamina after n cycles, while $S_{r,21}(n)$ and $S_{r,23}(n)$ are the residual shear strengths. The item $P_{\varphi,t(c)}/S_{r,\varphi}(n)$ can be calculated by the following relation with inclination parameters and shear strengths:

$$\frac{P_{\varphi,t(c)}}{S_{r,\varphi}(n)} = \frac{P_{23,t(c)}}{S_{r,23}(n)}\frac{\tau^2_{nt}(\theta)}{\tau^2_{n1}(\theta)+\tau^2_{nt}(\theta)} + \frac{P_{21,t(c)}}{S_{r,21}(n)}\frac{\tau^2_{n1}(\theta)}{\tau^2_{n1}(\theta)+\tau^2_{nt}(\theta)} \tag{5}$$

where the inclination parameters $P_{21,t}$, $P_{21,c}$, $P_{23,t}$ and $P_{23,c}$ take the empirical values given in Ref. [32]. As displayed in Fig. 1, θ represents the angle of the action plane. $\sigma_n(\theta)$, $\tau_{nt}(\theta)$ and $\tau_{n1}(\theta)$ are the stress components acting on the action plane:

$$\begin{cases} \sigma_n(\theta) = \sigma_{22}\cos^2\theta + \sigma_{33}\sin^2\theta + 2\tau_{23}\sin\theta\cos\theta \\ \tau_{nt}(\theta) = (\sigma_{33}-\sigma_{23})\sin\theta\cos\theta + \tau_{23}\left(\cos^2\theta - \sin^2\theta\right) \\ \tau_{n1}(\theta) = \tau_{31}\sin\theta + \tau_{21}\cos\theta \end{cases} \tag{6}$$

2.2. Constitutive equation with damage variable

Damage variables are generally introduced to characterize the damage initiations and propagations of the single lamina in damage mechanics. In this paper, the fiber tensile and compressive failures are captured by introducing the damage variables d_{fft} and d_{ffc}, respectively. d_{ifft} and d_{iffc} are adopted to characterize the tensile and compressive transverse inter-fiber failure. The constitutive equations with damage variables can be updated by Murakami-Ohno [33] theory: $\boldsymbol{\omega} = \sum \omega_k \boldsymbol{n}_k \otimes \boldsymbol{n}_k, k = (1,2,3)$, where$\omega_k$ and$\boldsymbol{n}_k$ are the principal damage variable and unit vector, respectively. To introduce damage into the constitutive equations, the damage variables d_{fft}, d_{ffc}, d_{ifft} and d_{iffc} related to the fracture angle θ_{fp} should be converted to the principle damage variables, thus a transform relation in terms of θ_{fp} needs to be established. In this paper, the principal damage variables can be obtained as follows:

$$\begin{cases} \omega_1 = \max\left(d_{fft}, d_{ffc}\right) \\ \omega_2 = \max\left(d_{ifft}, d_{iffc}\right)\cos^2\left(\theta_{fp}\right) \\ \omega_3 = \max\left(d_{ifft}, d_{iffc}\right)\sin^2\left(\theta_{fp}\right) \end{cases} \tag{7}$$

The damaged constitutive equations $C(\omega)$ can be expressed by the intact stiffness component and the principal damage variable ω_k as follows:

$$C(w) = \begin{bmatrix} d_1^2C_{11} & d_1d_2C_{12} & d_1d_3C_{13} & 0 & 0 & 0 \\ & d_2^2C_{22} & d_2d_3C_{23} & 0 & 0 & 0 \\ & & d_3^2C_{33} & 0 & 0 & 0 \\ & SYM & & d_{12}C_{44} & 0 & 0 \\ & & & & d_{13}C_{55} & 0 \\ & & & & & d_{23}C_{66} \end{bmatrix} \tag{8}$$

where $d_1 = 1-\omega_1, d_2 = 1-\omega_2, d_3 = 1-\omega_3$, $d_{12} = \left(\frac{2d_1d_2}{d_1+d_2}\right)^2, d_{13} = \left(\frac{2d_1d_3}{d_1+d_3}\right)^2, d_{23} = \left(\frac{2d_2d_3}{d_2+d_3}\right)^2$.

2.3. Damage evolution after damage initiation

Once any one failure criterion is activated, the material properties statically degrade following the damage evolution model. Because the internal failure inside laminated composites is mainly brittle fracture, the exponential damage evolution model [34] is employed to capture the sudden degradation of material properties. The damage variable can be calculated by equivalent displacements:

$$d_k = 1-\exp\left[\lambda_k\left(1-\delta_{eq,k}\Big/\delta^i_{eq,k}\right)\right]\delta^i_{eq,k}\Big/\delta_{eq,k}, k = \{fft, ffc, ifft, iffc\} \tag{9}$$

where $\delta^i_{eq,k}$ denotes the initial equivalent displacement when $\varphi_k = 1$ as illustrated in Fig. 2. The parameter λ_k governs the exponential softening and needs to be calculated through the fracture toughness $G_{C,k}$ related to each damage mode:

$$\lambda_k = 2\sigma^i_{eq,k}\delta^i_{eq,k}\Big/\left(2G_{C,k}-\sigma^i_{eq,k}\delta^i_{eq,k}\right), k = \{fft, ffc, ifft, iffc\} \tag{10}$$

where $\sigma^i_{eq,k}$ is the initial equivalent stress when $\varphi_k = 1$. In actual calculations, the initial equivalent stress and displacement can be obtained by multiplying the instantaneous $\sigma_{eq,k}$ and $\delta_{eq,k}$ by a scaling function $f_{sc,k}$:

$$\sigma^i_{eq,k} = \sigma_{eq,k}f_{sc,k};\ \delta^i_{eq,k} = \delta_{eq,k}f_{sc,k}, k = \{fft, ffc, ifft, iffc\} \tag{11}$$

The specific expressions of scaling function, equivalent displacements and stresses of each failure mechanism are presented in Table 1, where l_c denotes characteristic element length.

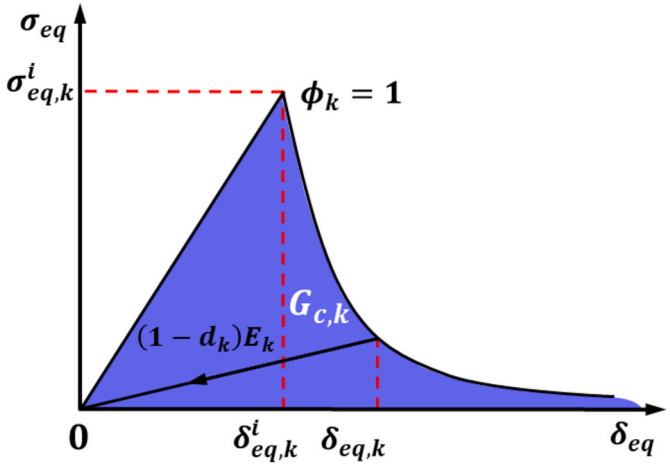

Fig. 2. The exponential damage evolution model for unidirectional lamina.

2.4. Gradual degradation of stiffness and strength

2.4.1. Residual stiffness degradation

For most fiber-reinforced composites, the residual stiffness exhibits a three-stage degradation trend. During stage I, the stiffness degrades rapidly in the first few cycles, then the stiffness decreases at a steady growth rate in stage II. Eventually, the stiffness reduces rapidly again and the final fracture occurs in stage III. Shiri et al. [35] introduced trigonometric terms to simulate the nonlinear decreasing trend of stiffness degradation as follows:

$$D_E(\mathrm{n}) = \frac{E_0 - E_r(\mathrm{n})}{E_0 - \sigma_{\max}/\varepsilon_f} = \frac{\sin(qx)\cos(q-p)}{\sin q\cos(qx-p)} \tag{12}$$

where E_0 and $E_r(\mathrm{n})$ denote the initial and residual stiffness related to the first cycle and the n_{th} cycle, respectively. $\sigma_{\max}$ is the maximum stress and the failure strain is assumed to be $\varepsilon_f = S_0/E_0$. Note that $x = n/N_f$, where n denotes the applied cycle and N_f denotes fatigue life. $D_E(\mathrm{n})$ is the stiffness degradation index whose value varies from 0 to 1, p and q are material parameters.

2.4.2. Residual strength degradation

The more complex the residual strength model, the more experimental efforts are required. Moreover, the residual strength of composites presents a large scatter. Complex models generally cannot guarantee more accurate simulated results, thus the simple models requiring less experimental data are an efficient choice for depicting the residual strength degradation. In this paper, similar to the approach for the residual stiffness, a trigonometric expression proposed by Lian [16] is adopted to define the strength degradation index.

$$D_S(n) = \frac{S_0 - S_r(n)}{S_0 - \sigma_{\max}} = \frac{\sin(\beta x)\cos(\beta-\alpha)}{\sin\beta\cos(\beta x-\alpha)} \tag{13}$$

where S_0 and $S_r(n)$ are the initial and residual strengths, respectively. $D_S(n)$ is the strength degradation index whose value varies from 0 to 1, β and α are material parameters and recommended to be $2\pi/3$ and $\pi/3$ if no experimental results are available [16].

2.4.3. Effective number of cycles

It is noted that the material degradation will result in stress redistribution inside the composite laminates, thus each element may be subjected to a variable amplitude fatigue load. It is therefore necessary to recalculate N_f in a new cycle, and the stresses and $x = n/N_f$ in the stiffness and strength degradation formulas are changing from cycle to cycle. To account for the nonlinear damage accumulation of variable amplitude cyclic loads, the concept of effective number of cycles [36] is

Table 1
The equivalent displacement, equivalent stress and scaling function for each failure mechanism based on the exponential damage model from Ref. [34].

Failure	$\delta_{eq,k}$	$\sigma_{eq,k}$	Scaling function
fft	$l_c\varepsilon_{11}$	$l_c\varepsilon_{11}\sigma_{11}/\delta_{eq,fft}$	$f_{sc,fft} = 1/\varphi_{fft}$
ffc	$l_c\lvert\varepsilon_{11}\rvert$	$l_c\lvert\varepsilon_{11}\sigma_{11}\rvert/\delta_{eq,ffc}$	$f_{sc,ffc} = 1/\varphi_{ffc}$
ifft	$l_c\sqrt{\varepsilon_n^2+\gamma_{nt}^2+\gamma_{n1}^2}$	$\frac{l_c(\sigma_n\varepsilon_n+\tau_{nt}\gamma_{nt}+\tau_{n1}\gamma_{n1})}{\delta_{eq,ifft}}$	$f_{sc,ifft} = (\sqrt{L^2+4Q}-L)/2Q$
	$L = \frac{2P_{\varphi,t}\sigma_n(\theta)}{S_{r,\varphi}(n)}$, $Q = \left(\frac{\sigma_n^2(\theta)}{[S_{r,2t}(n)]^2} - \frac{2P_{\varphi,t}\sigma_n^2(\theta)}{S_{r,\varphi}(n)S_{r,2t}(n)}\right) + \left(\frac{\tau_{nt}(\theta)}{S_{r,23}(n)}\right)^2 + \left(\frac{\tau_{n1}(\theta)}{S_{r,21}(n)}\right)^2$		
iffc	$l_c\sqrt{\gamma_{nt}^2+\gamma_{n1}^2}$	$\frac{l_c(\tau_{nt}\gamma_{nt}+\tau_{n1}\gamma_{n1})}{\delta_{eq,iffc}}$	$f_{sc,iffc} = (\sqrt{L^2+4Q}-L)/2Q$
	$L = 2P_{\varphi,c}\sigma_n(\theta)/S_{r,\varphi}(n)$, $Q = [\tau_{nt}(\theta)/S_{r,23}(n)]^2 + [\tau_{n1}(\theta)/S_{r,21}(n)]^2$		

adopted in this paper. As illustrated in Fig. 3, the effective number of cycles (n_{eff}) is defined as the number of fatigue cycles required to produce the same strength degradation in stress level 2 as occurs in stress level 1, which can be easily described by the relation: $D_{S_2}(n_{eff}) = D_{S_1}(n_1)$. The residual strength is selected as fatigue damage index and n_{eff} can be calculated as follows:

$$\frac{S_0 - S_r(\mathrm{i}-1)}{S_0 - \sigma_{\max}(\mathrm{i})} = \frac{\sin(\beta x_{eff})\cos(\beta-\alpha)}{\sin\beta\cos(\beta x_{eff}-\alpha)} \tag{14}$$

where $S_r(\mathrm{i}-1)$ represents the residual strength of the previous cycle, $\sigma_{\max}(\mathrm{i})$ denotes the maximum stress of the current cycle, and $x_{eff} = n_{eff}/N_f(\mathrm{i})$. The dichotomy method is adopted to calculate x_{eff}, which varies from 0 to 1. Only a few iterations are required to obtain the exact solution. Then the residual strength $S_r(\mathrm{i})$ and stiffness $E_r(\mathrm{i})$ of the current cycle can be obtained as follows:

$$\begin{cases} S_r(\mathrm{i}) = S_0 - [S_0 - \sigma_{\max}(\mathrm{i})]\dfrac{\sin[\beta x(\mathrm{i})]\cos(\beta-\alpha)}{\sin\beta\cos[\beta x(\mathrm{i})-\alpha]} \\ E_r(\mathrm{i}) = E_0 - [\mathrm{E}_0 - \sigma_{\max}(\mathrm{i})/\varepsilon_f]\dfrac{\sin[qx(\mathrm{i})]\cos(q-p)}{\sin q\cos[qx(\mathrm{i})-p]} \end{cases} \tag{15}$$

where $x(\mathrm{i}) = x_{eff} + \Delta n(\mathrm{i})/N_f(\mathrm{i})$, $\Delta n(\mathrm{i})$ represents the cyclic jump of each fatigue increment, $N_f(\mathrm{i})$ denotes the fatigue life under current stress state.

2.5. Normalized fatigue life model

In this study, the normalized fatigue life model [37] is employed to determine the fatigue life of unidirectional composites under arbitrary stress conditions:

$$\mu = \frac{\ln(a/f)}{\ln[(1-b)(c+b)]} = A + B\lg N_f \tag{16}$$

where $a = (\sigma_{\max} - \sigma_{\min})/2S_t, b = (\sigma_{\max} + \sigma_{\min})/2S_t, c = S_c/S_t$, S_t and S_c represent the static tension and compression strengths, respectively. $f = 1.06$, μ, A and B are curve fitting parameters derived from experimental results. In the case of shear loading, the positive and negative stress present the same effect on the fatigue life of composites, thus the parameter c in the above equation should be equal to 1. In addition, the logarithmic processing on the left side of Eq (16) is more consistent with experimental results, thus the normalized fatigue life model has been modified as follows:

$$\mu_{shear} = \lg\left(\frac{\ln(a/f)}{\ln[(1-b)(1+b)]}\right) = A_{shear} + B_{shear}\lg N_f \tag{17}$$

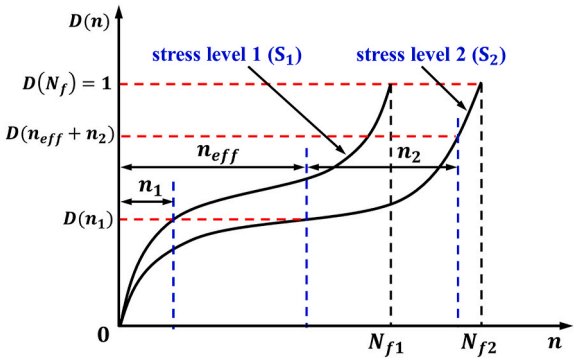

Fig. 3. Effective number of cycles under variable amplitude cyclic loadings.

3. Numerical implementation

3.1. Viscous regularization and tangent constitutive tensor

Note that damage degradation usually brings serious convergence difficulties to implicit numerical algorithms. To improve the convergence difficulty, the Duvaut-Lions viscous regularization [38] is carried out. Based on the viscous model, the time derivative of damage variable can be expressed as:

$$\dot{\omega}_k^v = \left(\omega_k - \omega_k^v\right)/\eta, (k=1,2,3) \tag{18}$$

where η indicates the viscous coefficient controlling the relaxation time of calculations. ω_k^v is the viscosity-regularized damage variable, which can be calculated by a backward-Euler method:

$$\omega_{k,i}^v = \left(\Delta t_i\omega_{k,i} + \eta\omega_{k,i-1}^v\right)/\left(\eta + \Delta t_i\right), (k=1,2,3) \tag{19}$$

where $\omega_{k,i}^v$ and $\omega_{k,i-1}^v$ denote the viscosity-regularized damage variables at the i_{th} and $(i-1)_{th}$ increments, respectively. Δt_i denotes the incremental time of the i_{th} increment. In addition, it is critical to precisely update the tangent constitutive tensor to guarantee a fast convergence rate of nonlinear iterative algorithms:

$$\dot{\boldsymbol{\sigma}} = \mathbf{C}_T\dot{\boldsymbol{\varepsilon}} \Rightarrow \mathbf{C}_T = \mathbf{C}(\omega) + \left[\sum_k \frac{\partial \mathbf{C}(\omega)}{\partial\omega_k^v}\frac{\partial\omega_k^v}{\partial\omega_k}\frac{\partial\omega_k}{\partial\boldsymbol{\varepsilon}}\right] : \boldsymbol{\varepsilon}, (k=1,2,3) \tag{20}$$

3.2. Representative volume cell (RVC)

The computational costs are related to the degrees of freedom of finite element models, thus reducing the size of the RVC is significant for numerical calculations. Moreover, it is necessary to guarantee that the thickness of the RVC is consistent with that of actual specimens (2.4 mm). For convenience, the width and length of the RVC are set equal to the thickness. As a result, a RVC model with the dimension of 2.4*2.4*2.4 mm^3 is constructed, as shown in Fig. 4. Two elements are partitioned for each single layer in the through-thickness direction. The local orientations of the layers rendered with different colors are 45, -45, 0 and 90°, respectively. Moreover, rational periodic boundary condition (PBC) has to be applied to the RVC so that it could represent the properties of the overall laminates. According to Li [39], the displacement equation constraints need to be imposed to the corresponding node pairs of face *A* and face *B*, face *C* and face *D* as follows.

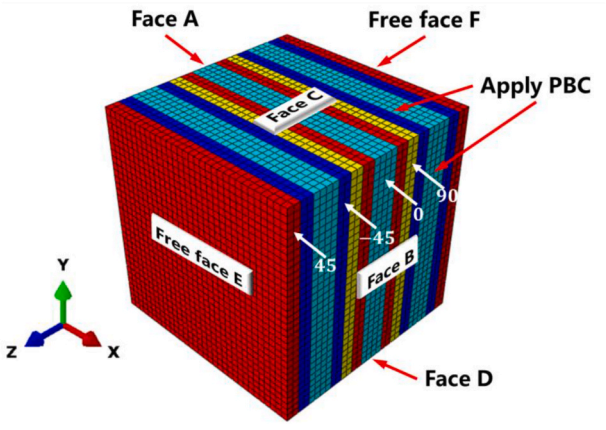

Fig. 4. Representative volume cell of composite laminates with periodic boundary conditions.

$$\begin{cases} Face\ A \Leftrightarrow B: \begin{cases} u_i(B) - u_i(A) = 2.4 \times \varepsilon_x^0 \\ v_i(B) - v_i(A) = 0 \\ w_i(B) - w_i(A) = 0 \end{cases} \\ Face\ C \Leftrightarrow D: \begin{cases} u_i(C) - u_i(D) = 2.4 \times \gamma_{xy}^0 \\ v_i(C) - v_i(D) = 2.4 \times \varepsilon_y^0 \\ w_i(C) - w_i(D) = 0 \end{cases} \end{cases} \tag{21}$$

where u_i, v_i and w_i are the displacements at specific nodes, ε_x^0, ε_y^0 and γ_{xy}^0 are the global average strains of the RVC. The thickness of RVC is equal to that of actual specimens, thus it is not necessary to assign PBC to face *E* and face *F*.

3.3. Fatigue loading with different cyclic jump algorithms

Two analysis steps are required to apply fatigue loading to the RVC model as illustrated in Fig. 5. The first analysis step is a static step, which increases the external load form 0 to the maximum fatigue stress σ_{max}. **Step 2** is a fatigue analysis step, in which the external load is always maintained at σ_{max}. Owing to the assumption that the damage is most likely to initiate when the fatigue stress reaches σ_{max}, each increment in **step 2** represents a cyclic loading. It should be noted that in numerical calculations, it is impractical to update the damage status of the RVC cycle by cycle due to the huge computational cost. To balance the accuracy of life predictions and computational efficiency, it is critical to choose the cyclic jump appropriately. A large cycle jump is desirable to reduce the computation time, but is not able to correctly capture the rapid material degradations that occur near the end of fatigue life. Therefore, it is desirable to adaptively change the cycle jump depending on the damage growth rate. Instead of determining the damage growth rate directly, the cycle jump can be tied to the numerical increment time

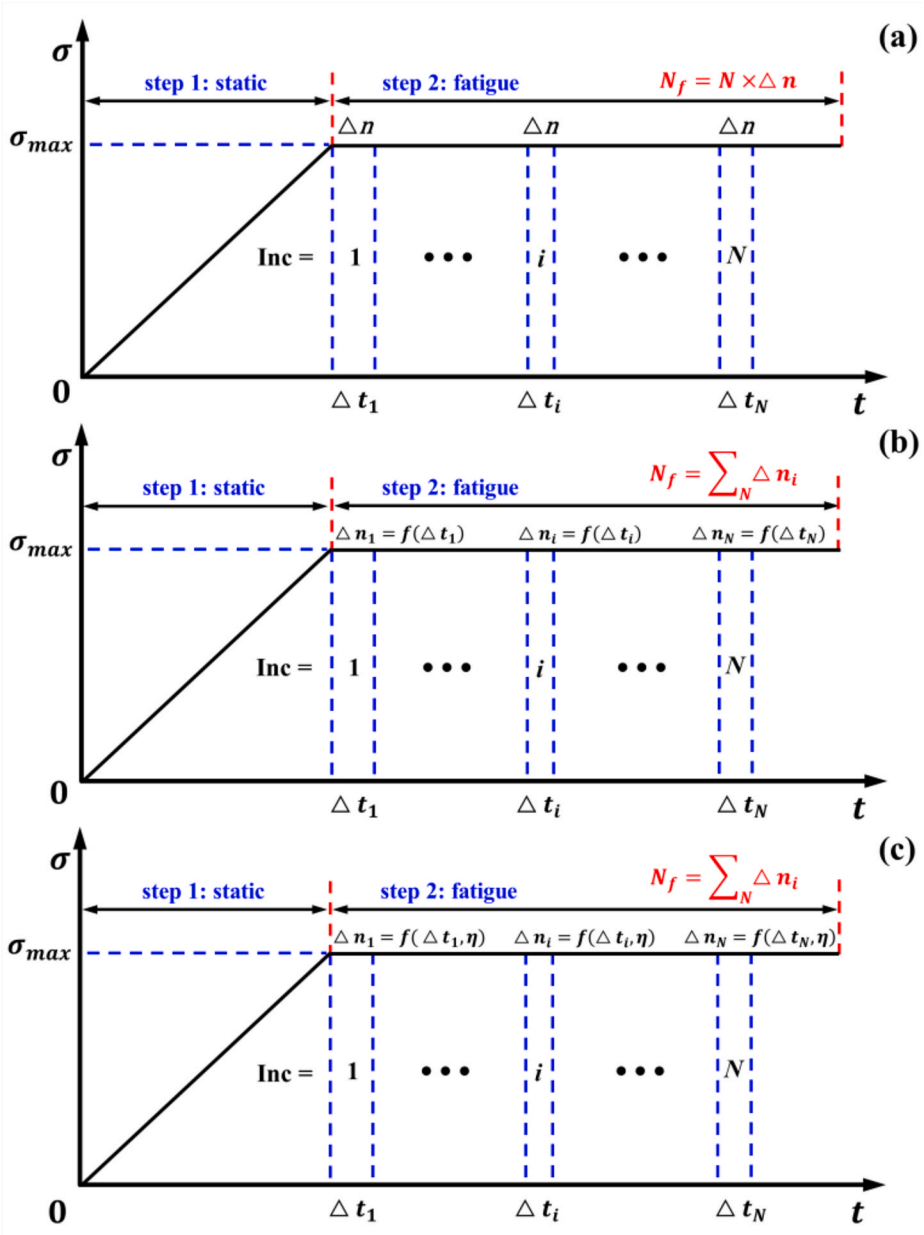

Fig. 5. Illustration of fatigue loadings of the RVC model with different cyclic jump algorithms: (a) **algorithm A**, (b) **algorithm B**, (c) **algorithm C**.

Δt_i, as the FE code will automatically reduce the increment time to deal with the convergence difficulties created by rapid damage growth.

Three different cyclic jump algorithms are separately employed to predict the fatigue lives of composites. As indicated in Fig. 5, **algorithm A** adopts a constant cyclic jump for each increment, which is the most commonly used method in the literature [23–25]. However, this method generally results in a great sensitivity to the choice of increment according to Guo et al. [24]. In contrast to employing constant a cyclic jump in **algorithm A**, **algorithm B,** shown in Fig. 5(b), introduces an adaptive and time-dependent cyclic jump approach. Due to the convergence difficulties of iterative algorithms, especially when damage grows, the convergence rate in **step 2** will change continuously. In the actual calculations of Abaqus/Standard, the incremental time Δt_i will be automatically reduced to a quarter of the previous increment if convergence difficulties are encountered, and Δt_i will be automatically increased by a half of the previous increment if the convergence rate is fast. As a result, Δt_i may even drop to a small magnitude ($10^{-6} - 10^{-5}$) at some increments during the calculations, especially near the final rupture of the RVC model. For these increments with small Δt_i, a constant cyclic jump may increase the chances of overshooting the point at which sudden failure occurs. In view of this situation, the cyclic jump Δn_i of **algorithm B** is defined to be related to Δt_i:

$$\Delta n_i = Dn * \Delta t_i / \Delta t_{scale} \tag{22}$$

where $\Delta t_{scale} = 0.005$ is a timescale parameter for dimensionless the Δt_i, and Dn is the cyclic jump parameter, whose effect on life predictions will be discussed in section 5.3. In addition, to solve the convergence problems, it is necessary to introduce a viscous coefficient to regularize the damage variable, as stated in section 3.1. According to Eq. (19), the actual damage increment at the i_{th} increment can be obtained through the following derivations:

$$\Delta\omega_{k,i} = \omega^v_{k,i} - \omega^v_{k,i-1} = \frac{\Delta t_i \omega_{k,i} + \eta \omega^v_{k,i-1}}{\eta + \Delta t_i} - \omega^v_{k,i-1} = \left(\omega_{k,i} - \omega^v_{k,i-1}\right)\frac{\Delta t_i}{\eta + \Delta t_i} = D\omega_{k,i}\frac{\Delta t_i}{\eta + \Delta t_i} \tag{23}$$

It can be seen from Eq. (23) that the viscous coefficient η has a certain influence on the actual damage developments. The incremental damage $D\omega_{k,i}$ needs to be viscosity regularized by multiplying by $\Delta t_i/(\eta + \Delta t_i)$. Therefore, it seems more reasonable to correlate the cyclic jump Δn_i with both Δt_i and η. Consequently, the cyclic jump of **algorithm C** is defined as follows:

$$\Delta n_i = Dn * \Delta t_i / \Delta t_{scale} * \Delta t_i / (\eta + \Delta t_i) \tag{24}$$

When implementing the adaptive cyclic jump algorithms, there is no need to collect the information of all integration points and no extrapolation method is used, which effectively avoids the extrapolation error in life predictions. The sensitivity of life predictions to the cyclic jump parameter Dn of the three models will be evaluated and compared in detail in section 5.3.

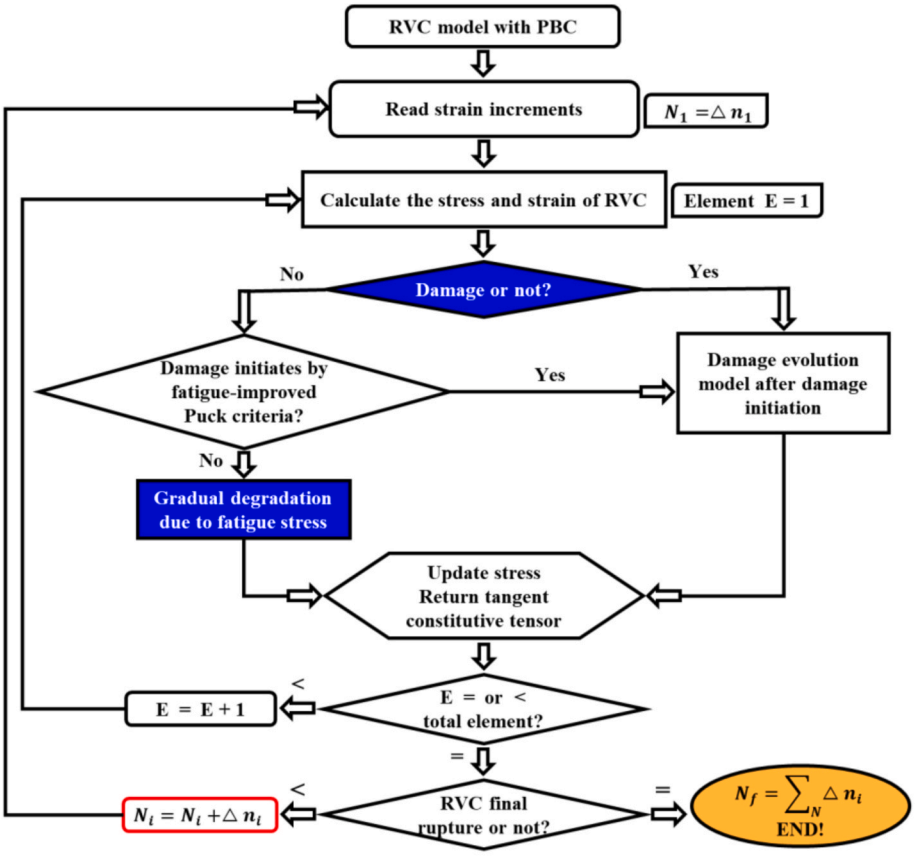

Fig. 6. The numerical computation procedure of the progressive fatigue damage model.

3.4. Numerical computation procedure

The numerical computation procedure of the fatigue damage model is briefly presented in Fig. 6. As can be seen, the calculation process starts with the RVC model preparation. After calculating the stress and strain components, the fatigue-improved Puck criterion is employed to identify whether fatigue damage has initiated or not. If damage initiates, the corresponding stiffness decreases sharply following the sudden degradation rules, otherwise the element properties will gradually degrade with the increasing number of fatigue cycles. After N incremental iterations, the final rupture of RVC occurs and the predicted life can be obtained through $N_f = \sum_N \Delta n_i$. The fatigue life predictions are conducted in Abaqus/Standard by incorporating a user defined subroutine UMAT.

4. Experiments and model input parameters

One set of experiments were conducted to obtain the material parameters required by the fatigue damage model, including quasi-static and fatigue tests on unidirectional laminates with $[0]_{16}$, $[(45/-45)_8]$ and $[90]_{16}$ lay-ups. Another set of experiments on multidirectional laminates with $[45/-45/0/0/-45/90/45/0]_S$ lay-up was conducted to validate the accuracy of simulated results.

4.1. Quasi-static and fatigue experiment

As shown in Fig. 7, Quasi-static and fatigue experiments were conducted on a MTS 370 testing machine. The ultimate failure strengths were obtained under displacement-controlled method and the loading rate was 0.5 mm/min. The tension-tension and compression-compression fatigue tests were performed under sine wave load-controlled method, and the frequency was chosen between 5 and 10 Hz to ensure the temperature did not rise by more than 10 °C during the test. The schematic diagrams of the specimens are illustrated in Fig. 7. The nominal dimensions of the tensile specimen were 250 × 25 × 2.4 mm^3, while the dimensions of the compressive specimens were designed as 126 × 25 × 2.4 mm^3. Aluminum tabs with 1.5 mm thickness and 56 mm length were glued on the ends of all specimens. The stress ratios R were set to be 0.1 for tensile fatigue test and 10 for compressive fatigue test. The maximum absolute fatigue stress levels were defined as a percentage of failure strengths measured from the quasi-static experiments.

4.2. Material properties of unidirectional lamina

The material properties of the T800 carbon/bismaleimide unidirectional composite are summarized in Table 2, which were measured from the tests on $[0]_{16}$, $[90]_{16}$ and $[(45/-45)_8]$ specimens. The fiber volume fraction of UD ply is 58%. Due to the absence of experimental data, the fracture toughness $G_{C,k}$ are taken from the literature [40]. The Poisson's ratio ν_{23} and shear modulus G_{23} are difficult to obtain through experiments. They were therefore calculated based on the transversely isotropic assumption according to the following relations:

Table 2
Material properties of T800 carbon/bismaleimide unidirectional composite.

Parameters	Symbols	Mean value
Longitudinal & transverse elastic modulus	$E_{11}/E_{22},E_{33}$	172.02/9.62 GPa
In-plane & out-plane shear modulus	$G_{12},G_{13}/G_{23}$	9.90/3.36 GPa
Poisson's ratio	$\nu_{12},\nu_{13}/\nu_{23}$	0.31/0.43
Longitudinal tensile & compressive strength	S_{1t}/S_{1c}	2640.7/1122.1 MPa
Transverse tensile & compressive strength	S_{2t}/S_{2c}	78.3/164.4 MPa
In-plane & out-plane shear strength	$S_{12},S_{13}/S_{23}$	88.6/61.9 MPa
Longitudinal fracture toughness [40]	$G_{C,fft}/G_{C,ffc}$	121.4/76.5 N/mm
Transverse fracture toughness	$G_{C,ifft}/G_{C,iffc}$	0.46/1.38 N/mm

$$\begin{cases} E_{33} = E_{22}, \nu_{13} = \nu_{12}, G_{13} = G_{12} \\ \nu_{23} = \dfrac{\nu_{12}(1-\nu_{12}E_{22}/E_{11})}{1-\nu_{12}}, G_{23} = \dfrac{E_{22}}{2(1+\nu_{23})} \\ S_{12} = S_{13}, S_{23} = S_{2c}/[2\tan(53^\circ)] \end{cases} \tag{25}$$

4.3. Normalized fatigue life curves

The normalized fatigue life curves in longitudinal, transverse and in-plane shear directions of unidirectional composites were extracted from the fatigue experiments on $[0]_{16}$, $[90]_{16}$ and $[(45/-45)_8]$ specimens, respectively. The 'μ' values under different loading conditions were calculated according to Eq. (16). As displayed in Fig. 8, the normalized fatigue life curves in three different directions can be determined by regarding μ and logarithmic life $\log(N_f)$ as the ordinate and abscissa, respectively, and the material parameters are presented in Table 3.

4.4. Stiffness and strength degradation rules

Fatigue experiments on $[(45/-45)_8]$ and $[0]_{16}$ specimens were performed to characterize the stiffness degradation rules. The residual stiffness was measured at each designated cycle by conducting a tensile experiment without destroying the specimens, and the experiment was conducted on the same machine in quasi-static loading under load control. The normalized stiffness degradation curves are presented in Fig. 9(a). Given the limited number of specimens, it was assumed that

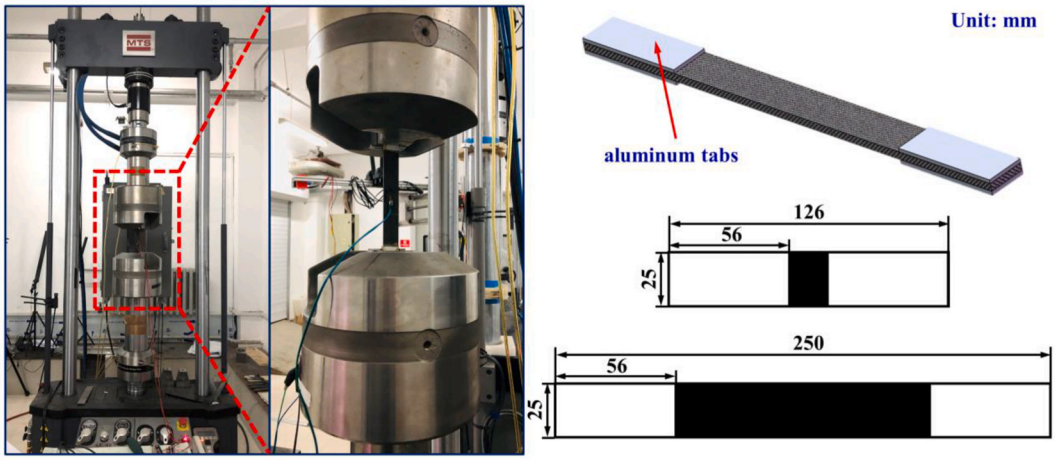

Fig. 7. MTS 370 servo-hydraulic testing machine and the schematic diagrams of specimens.

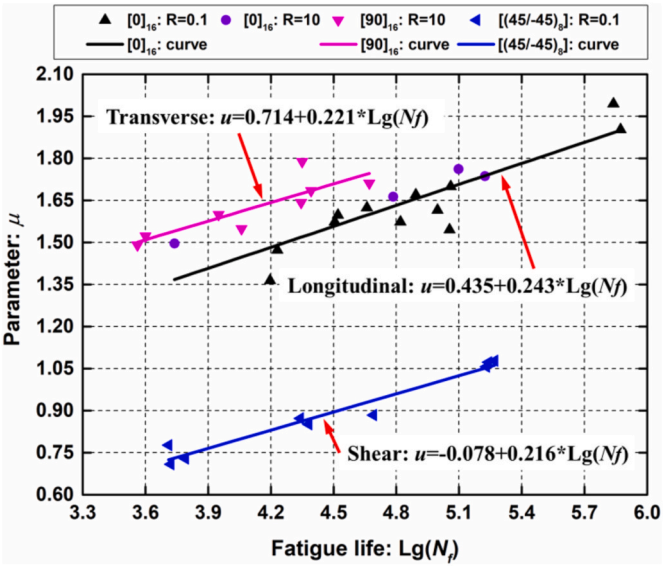

Fig. 8. Normalized fatigue life curves in longitudinal, transverse and shear directions of unidirectional composites.

Table 3
Material parameters of normalized fatigue life curves in different directions for a UD ply.

Fitting parameters	*A*	*B*
Longitudinal direction	0.435	0.243
Transverse direction	0.714	0.221
In-plane shear direction	−0.078	0.216

the stiffness in transverse direction possesses the same degradation rule as that in longitudinal direction. Fatigue failure experiments on $[(45/-45)_8]$ specimens were also performed to determine the strength degradation rules. The normalized strength degradation curve for in-plane shear is illustrated in Fig. 9(b). The experimental data are well covered by the fitting curve and the fitting parameters are summarized in Table 4.

5. Results and discussion

5.1. Static strength and fatigue life prediction

As presented in Fig. 10, the stress-strain relation of multidirectional laminates with $[45/-45/0/0/-45/90/45/0]_S$ lay-up is simulated and compared with the experimental curves. The predicted elastic modulus and failure strength are slightly higher than the experimental values, but on the whole they are in good agreement. The predicted curve initially experiences a small linear growth segment, then the slope gradually decreases because of the development of internal damage. When the strain reaches 1.33%, the structure loses its load-bearing capacity and the reaction force suddenly drops to a very small value, indicating the

Table 4
The fitting parameters of residual stiffness and strength degradation rules.

Fitting parameters	*p*	*q*	*α*	*β*
Longitudinal direction	1.504	3.019	π/3	2π/3
In-plane shear direction	1.521	3.026	1.316	2.841
Transverse direction	1.504	3.019	π/3	2π/3

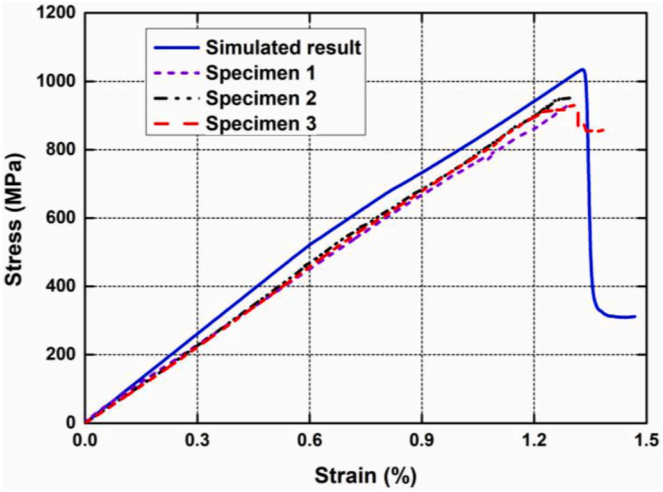

Fig. 10. Stress-strain curves of composite laminates under quasi-static tension loadings.

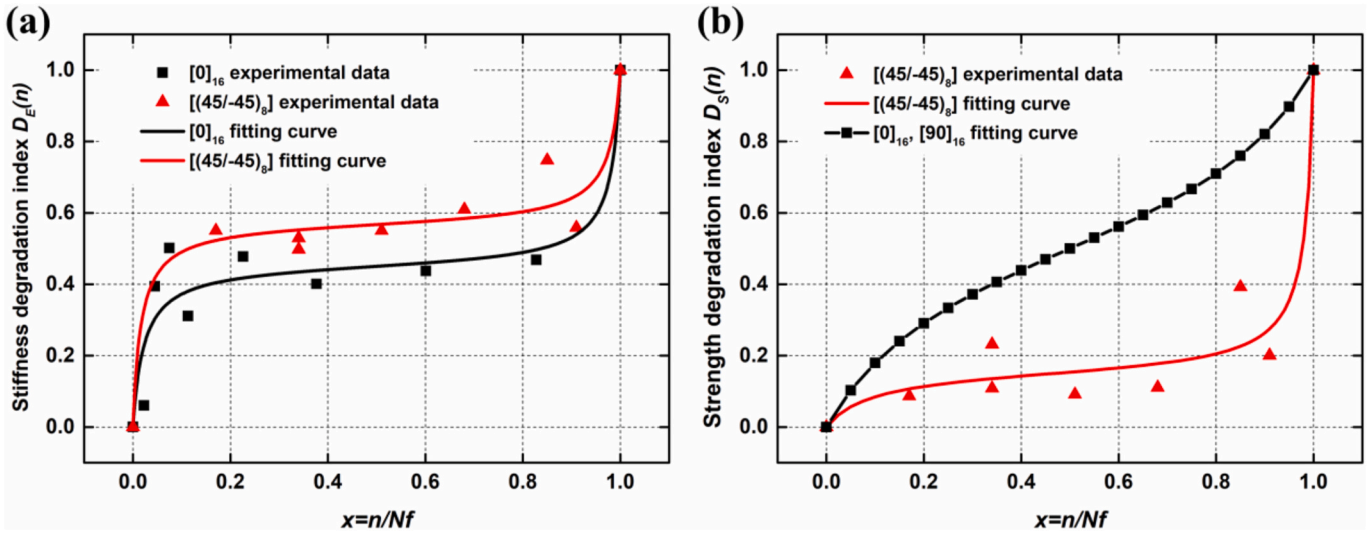

Fig. 9. (a) Normalized stiffness degradation curves and (b) strength degradation curves.

Table 5
The simulated and experimental modulus, failure strength and strain of laminates.

Properties	Modulus/GPa	Strength/MPa	Failure strain/%
Specimen 1	74.1	938.1	1.30
Specimen 2	80.6	951.0	1.29
Specimen 3	78.7	932.1	1.32
Mean value	77.8	940.4	1.30
Simulation	84.6	1034.6	1.33
Deviation/%	8.7	10.0	2.0

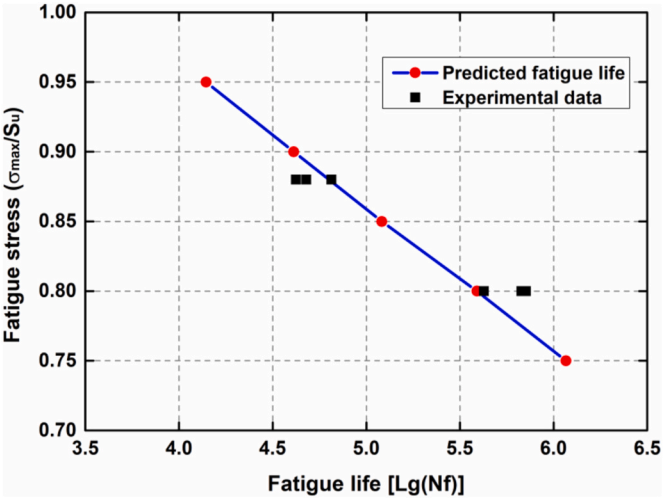

Fig. 11. Comparison between predicted lives and experimental data of multidirectional laminates under tension-tension fatigue loading.

brittle fracture of the composite. The simulated and experimental elastic modulus, strengths and failure strains of composite laminates are summarized in Table 5. The deviations between the predicted and experimental results of modulus, failure strength and strain are 8.7%, 10.0% and 2.0%, respectively.

The predicted fatigue lives of multidirectional laminates under tension fatigue loadings are displayed in Fig. 11, which are compared with the experimental results. The simulated fatigue stress levels varied from 0.75 to 0.95 of the static failure strength. With the increase of maximum fatigue stresses, the logarithmic fatigue life exhibits an approximate linear decreasing tendency. Different from the deterministic life obtained by the prediction, the experimental data exhibits certain scatter as shown in Fig. 11. Generally, the simulated fatigue lives correlate well with the experimental results.

5.2. Predicted residual stiffness curves

Fig. 12 presents the predicted residual stiffness curves of the multidirectional laminates under tension fatigue loading with different stress levels. It can be seen that all residual stiffness curves follow a similar three-stages degradation trend, which qualitatively matches the behavior seen experimentally for the unidirectional specimens (Fig. 9). The residual stiffness decreases rapidly at the initial stage of fatigue loading, and then decreases slowly in the intermediate stage which constitutes the vast majority of the whole fatigue period. Finally, the residual stiffness sharply decreases to a small magnitude, indicating that the composite loses its load-bearing capacity. Guo et al. [24] pointed out that it is necessary to define a standard for determining the material fatigue failure, since different magnitudes of stiffness degradation generally correspond to different cyclic numbers. In reference [24], 90%, 80%, and 50% residual stiffnesses were defined as the fatigue failure standards, and different simulated fatigue lives were obtained because the cyclic number still continues to increase in the final stage of fatigue loading. However, in this paper, the eventual material breakage occurs within a small number of cycles in the final stage, thus there is no need to artificially define a standard for determining the material failure in numerical calculations. It is noted that the smaller the fatigue stress levels, the more obvious the stiffness degradation tendency. This may be due to the fact that at lower stress level, the properties of composites need to degrade more to result in the eventual breakage, and more loading cycles are also required during the fatigue period.

5.3. Sensitivity of life predictions to cyclic jump

To reduce the sensitivity of life predictions to cyclic jump, three different cyclic jump algorithms are incorporated within the PFDM. The residual stiffness curves are predicted by the three different algorithms as presented in Fig. 13. The fatigue stress level in Fig. 13(a) and (c) are 85% and 90% of the static strength, respectively, and the cyclic jump parameter *Dn* is set sequentially from 100 to 1000. It can be seen that the stiffness degradations of all algorithms in the initial stage and intermediate stage are consistent as described in section 5.2. However, significant differences of residual stiffness curves in the final stage can be observed with the increasing *Dn* of **algorithm A**. The larger the cyclic

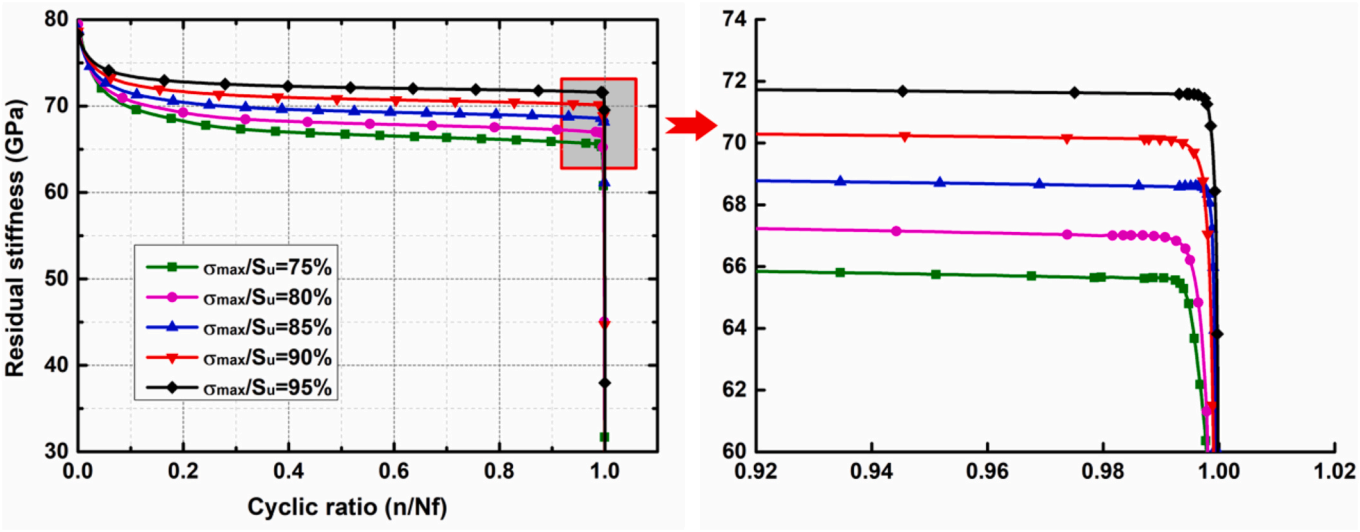

Fig. 12. Predicted residual stiffness curves of composite laminates under tension-tension fatigue loadings with varied stress levels.

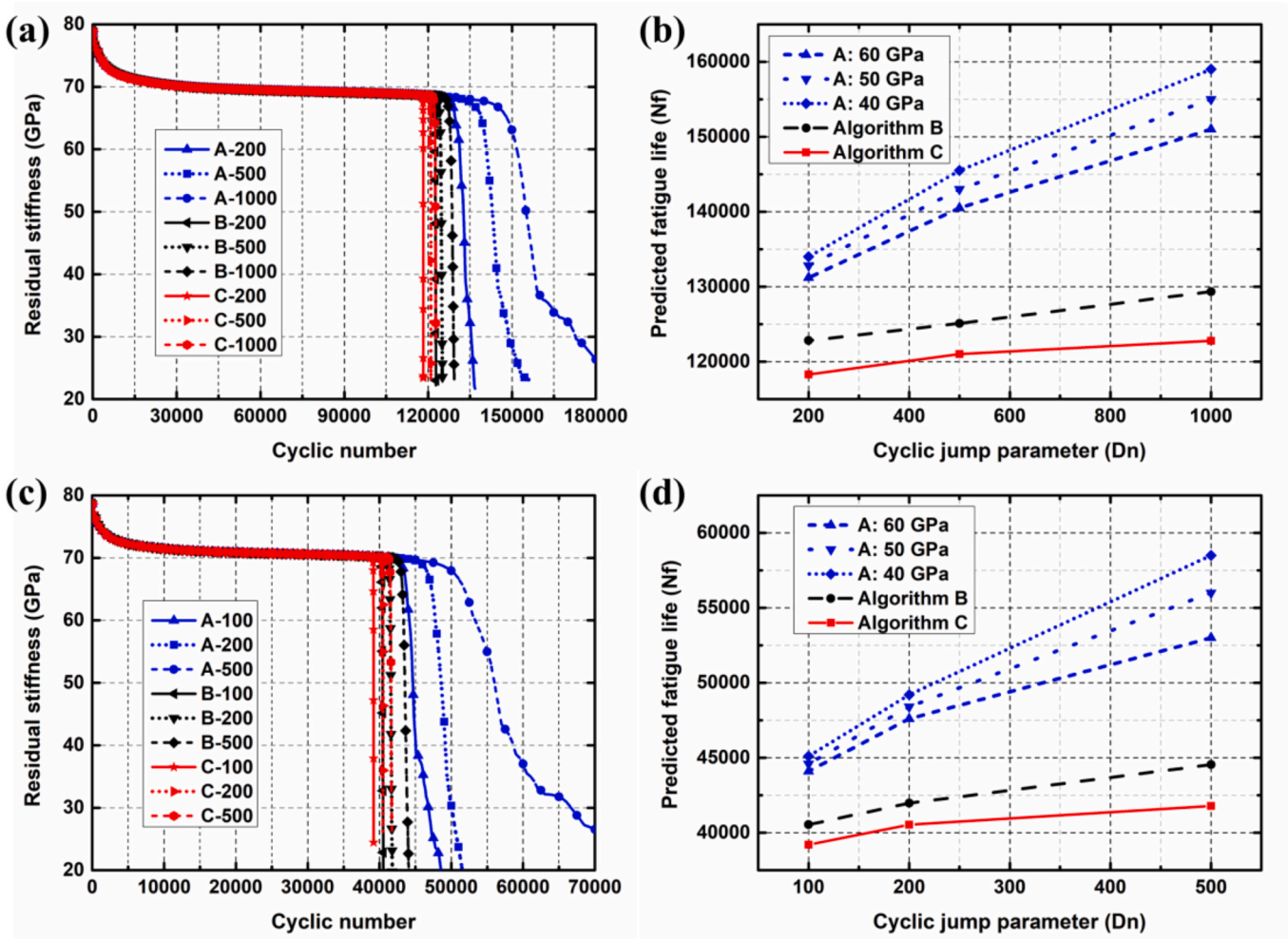

Fig. 13. Life predictions by different cyclic jump algorithms: (a) residual stiffness curves under 85% stress level and (b) relation between fatigue life and cyclic jump, (c) residual stiffness curves under 90% stress level and (d) relation between fatigue life and cyclic jump.

jump, the slower the rate of stiffness degradations. Moreover, when setting 60 GPa as the material failure standard, the fatigue lives of **algorithm A**n under 85% stress level are 131200, 140500 and 151000, respectively, but these fatigue lives become 134000, 145500, 159000 when 40 GPa is chosen as the failure standard. Therefore, the life predictions and stiffness degradations of **algorithm A** are sensitive to the user defined cyclic jump Δn.

As displayed in Fig. 13, the sensitivity of life predictions to cyclic jump parameter *Dn* has been greatly reduced by **algorithm B** and **algorithm C**. Residual stiffness curves decrease rapidly in the final stage, presenting a brittle-like fracture. Thus it is not necessary to artificially define a standard for determining the material failure. Although the predicted fatigue lives still increase slightly with the increasing *Dn*, the range of variation is quite limited. Moreover, by considering the influence of viscosity coefficient, the fatigue lives obtained by **algorithm C** are slightly lower than those obtained by **algorithm B**, and the variation range of fatigue life with the increasing *Dn* is also smaller. It should be noted that the total increments required for eventual breakage in **step 2**, which correlate to the required computation time, are negatively related to the cyclic jump parameter *Dn*. After the eventual breakage point, the residual stiffness of the RVC decreases rapidly. In the case of 90% fatigue stress, when *Dn* is selected as 100, 200, and 500, the required increments of **algorithm C** to reach the eventual breakage are 570, 309, and 159, respectively, while the predicted fatigue life barely changes. Therefore, in the numerical calculations, the cyclic jump parameter *Dn* of the **algorithm C** can be arbitrarily selected within a relatively large range to obtain convergent results, which ingeniously balances the accuracy of life predictions and computational efficiency.

6. Conclusions

In this work, the following conclusions can be drawn:

(1) A new progressive fatigue damage model, incorporating an adaptive cyclic jump algorithm, is proposed and applied to predict the failure strength, fatigue lives and residual stiffness curves of multidirectional composite laminates. The numerical predictions are compared with the available experimental results, and an overall good consistency is obtained.

(2) A parametrical study has been conducted to investigate the sensitivity of life predictions to three different cyclic jump algorithms. The life predictions and stiffness degradations are sensitive to the constant cyclic jump algorithm. The sensitivity of life predictions to cyclic jump parameter has been greatly reduced by correlating the cyclic jump with the increment time and viscous coefficient. The cyclic jump parameter of the adaptive algorithm can be arbitrarily selected within a relatively large range to obtain convergent results, which ingeniously balances the accuracy of life predictions and computational efficiency.

(3) Considering that the predicted residual stiffness decreases rapidly within small number cycles in the final stage when incorporating the adaptive cyclic jump algorithm, it is not necessary to define a

standard for determining the material failure in numerical calculations, which effectively eliminates an artificially induced uncertainty in life predictions.

Author statement

Tao Zheng: Conceptualization, Investigation, Methodology, Formal analysis, Software, Validation, Writing-Original Draft.

Licheng Guo: Supervision, Methodology, Writing - Review & Editing.

Rinze Benedictus: Supervision, Writing - Review & Editing.

John-Alan Pascoe: Supervision, Conceptualization, Writing - Review & Editing.

Zhenxin Wang: Methodology, Writing - Review & Editing.

Declaration of competing interest

The authors declare that they have no known competing financial interests or personal relationships that could have appeared to influence the work reported in this paper.

Acknowledgements

This work was supported by National Science and Technology Major Project (2017-VII-0011-0106), Natural Science Foundation of Heilongjiang Province (ZD2019A001), and China Scholarship Council (No.202006120106). The authors are grateful to Heilongjiang Touyan Innovation Team Program.

References

[1] C. Soutis, Carbon fiber reinforced plastics in aircraft construction, Mater. Sci. Eng., A 412 (1–2) (2005) 171–176.
[2] P. Gholami, M.A. Farsi, M.A. Kouchakzadeh, Stochastic fatigue life prediction of Fiber-Reinforced laminated composites by continuum damage Mechanics-based damage plastic model, Int. J. Fatig. 152 (2021), 106456.
[3] J. Degrieck, W. Van Paepegem, Fatigue damage modeling of fibre-reinforced composite materials: Review, Appl. Mech. Rev. 54 (4) (2001) 279–300.
[4] Z. Hashin, A. Rotem, A fatigue failure criterion for fiber reinforced materials, J. Compos. Mater. 7 (1973) 448–464.
[5] F. Ellyin, H. El-Kadi, A fatigue failure criterion for fiber reinforced composite laminae, Compos. Struct. 15 (1) (1990) 61–74.
[6] A.P. Vassilopoulos, B.D. Manshadi, T. Keller, Influence of the constant life diagram formulation on the fatigue life prediction of composite materials, Int. J. Fatig. 32 (4) (2010) 659–669.
[7] I.M. Daniel, A. Charewicz, Fatigue damage mechanisms and residual properties of graphite/epoxy laminates, Eng. Fract. Mech. 25 (5–6) (1986) 793–808.
[8] P.M. Barnard, R.J. Butler, P.T. Curtis, The Strength-Life Equal Rank Assumption and its application to the fatigue life prediction of composite materials, Int. J. Fatig. 10 (3) (1988) 171–177.
[9] H. Kawakami, T. Fujii, Y. Morita, Fatigue degradation and life prediction of glass fabric polymer composite under tension/torsion biaxial loading, J. Reinforc. Plast. Compos. 15 (2) (1996) 183–195.
[10] H.A. Whitworth, A stiffness degradation model for composite laminates under fatigue loading, Compos. Struct. 40 (2) (1998) 95–101.
[11] W. Yao, N. Himmel, A new cumulative fatigue damage model for fibre-reinforced plastics, Compos. Sci. Technol. 60 (1) (2000) 59–64.
[12] R.D.B. Sevenois, W. Van Paepegem, Fatigue damage modeling techniques for textile composites: Review and comparison with unidirectional composite modeling techniques, Appl. Mech. Rev. 67 (2) (2015), 020802.
[13] M.M. Shokrieh, L.B. Lessard, Progressive fatigue damage modeling of composite materials. part 1: Modeling, J. Compos. Mater. 34 (13) (2000) 1056–1080.
[14] X. Diao, L.B. Lessard, M.M. Shokrieh, Statistical model for multiaxial fatigue behavior of unidirectional plies, Compos. Sci. Technol. 59 (13) (1999) 2025–2035.
[15] K.I. Tserpes, P. Papanikos, G. Labeas, Sp Pantelakis, Fatigue damage accumulation and residual strength assessment of CFRP laminates, Compos. Struct. 63 (2) (2004) 219–230.
[16] W. Lian, W. Yao, Fatigue life prediction of composite laminates by FEA simulation method, Int. J. Fatig. 32 (1) (2010) 123–133.
[17] P. Shabani, F. Taheri-Behrooz, S. Maleki, M. Hasheminasab, Life prediction of a notched composite ring using progressive fatigue damage models, Compos. B Eng. 165 (2019) 754–763.
[18] J. Xiong, Y. Zhu, C. Luo, Y. Li, Fatigue-driven failure criterion for progressive damage modelling and fatigue life prediction of composite structures, Int. J. Fatig. 145 (2021), 106110.
[19] P. Shabani, N. Shabani, Fatigue life prediction of high-speed composite craft under slamming loads using progressive fatigue damage modeling technique, Eng. Fail. Anal. 131 (2022), 105818.
[20] G. Fang, J. Liang, B. Wang, Progressive damage and nonlinear analysis of 3D four-directional braided composites under unidirectional tension, Compos. Struct. 89 (1) (2009) 126–133.
[21] I. Lapczyk, J.A. Hurtado, Progressive damage modeling in fiber-reinforced materials, Composer Part A-Appl S 38 (11) (2007) 2333–2341.
[22] W. Van Paepegem, J. Degrieck, P. De Baets, Finite element approach for modelling fatigue damage in fibre-reinforced composite materials, Compos. B Eng. 32 (7) (2001) 575–588.
[23] J. Song, W. Wen, H. Cui, Fatigue life prediction model of 2.5D woven composites at various temperatures, Chin. J. Aeronaut. 31 (2) (2018) 310–329.
[24] J. Guo, W. Wen, H. Zhang, H. Cui, A mesoscale fatigue progressive damage model for 3D woven composites, Int. J. Fatig. 152 (2021), 106455.
[25] S. Zhou, Y. Li, K. Fu, X. Wu, Progressive fatigue damage modelling of fibre-reinforced composite based on fatigue master curves, Thin-Walled Struct. 158 (2021), 107173.
[26] J. Xu, S.V. Lomov, I. Verpoest, S. Daggumati, W. Van Paepegem, J. Degrieck, A progressive damage model of textile composites on meso-scale using finite element method: fatigue damage analysis, Comput. Struct. 152 (2015) 96–112.
[27] J.A. Rivera, E. Aguilar, D. Cárdenas, H. Elizalde, O. Probst, Progressive failure analysis for thin-walled composite beams under fatigue loads, Compos. Struct. 154 (2016) 79–91.
[28] J. Llobet, P. Maimí, Y. Essa, F. Martin de la Escalera, A continuum damage model for composite laminates: Part III – Fatigue, Mech. Mater. 153 (2021), 103659.
[29] O. Sally, F. Laurin, C. Julien, R. Desmorat, F. Bouillon, An efficient computational strategy of cycle-jumps dedicated to fatigue of composite structures, Int. J. Fatig. 135 (2020), 105500.
[30] A. Puck, H. Schürmann, Failure analysis of FRP laminates by means of physically based phenomenological models, Compos. Sci. Technol. 62 (2002) 1633–1662.
[31] H.M. Deuschle, B.-H. Kröplin, Finite element implementation of Puck's failure theory for fibre-reinforced composites under three-dimensional stress, J. Compos. Mater. 46 (19–20) (2012) 2485–2513.
[32] A. Puck, M. Kopp, M. Knops, Guidelines for the determination of the parameters in Puck's action plane strength criterion, Compos. Sci. Technol. 62 (2002) 371–378.
[33] M. Zako, Y. Uetsuji, T. Kurashiki, Finite element analysis of damaged woven fabric composite materials, Compos. Sci. Technol. 63 (3–4) (2003) 507–516.
[34] T. Zheng, L. Guo, J. Huang, G. Liu, A novel mesoscopic progressive damage model for 3D angle-interlock woven composites, Compos. Sci. Technol. 185 (2020), 107894.
[35] S. Shiri, M. Yazdani, M. Pourgol-Mohammad, A fatigue damage accumulation model based on stiffness degradation of composite materials, Mater. Des. 88 (2015) 1290–1295.
[36] J.R. Schaff, B.D. Davidson, Life prediction methodology for composite structures. Part II-spectrum fatigue, J. Compos. Mater. 31 (2) (1997) 158–181.
[37] T. Adam, G. Fernando, R.F. Dickson, H. Reiter, B. Harris, Fatigue life prediction for hybrid composites, Int. J. Fatig. 11 (4) (1989) 233–237.
[38] G. Duvaut, J.L. Lions, Inequalities in Mechanics and Physics, Springer, Berlin, 1976.
[39] S. Li, Boundary conditions for unit cells from periodic microstructures and their implications, Compos. Sci. Technol. 68 (9) (2008) 1962–1974.
[40] G. Fang, J. Liang, Q. Lu, B. Wang, Y. Wang, Investigation on the compressive properties of the three dimensional four-directional braided composites, Compos. Struct. 93 (2) (2011) 392–405.